

# Adenosine Deaminase Prefers a Distinct Sugar Ring Conformation for Binding and Catalysis: Kinetic and Structural Studies

Harry Ford, Jr., Fang Dai, Lan Mu, Maqbool A. Siddiqui, Marc C. Nicklaus, Lynne Anderson, Victor E. Marquez, and Joseph J. Barchi, Jr.\*

Laboratory of Medicinal Chemistry, Division of Basic Sciences, National Cancer Institute, 37 Convent Drive, MSC4255, Bethesda, Maryland 20892-4255

Received September 9, 1999; Revised Manuscript Received December 7, 1999

**ABSTRACT:** Several recent X-ray crystal structures of adenosine deaminase (ADA) in complex with various adenosine surrogates have illustrated the preferred mode of substrate binding for this enzyme. To define more specific structural details of substrate preferences for binding and catalysis, we have studied the ADA binding efficiencies and deamination kinetics of several synthetic adenosine analogues in which the furanosyl ring is biased toward a particular conformation. NMR solution studies and pseudorotational analyses were used to ascertain the preferred furanose ring puckers ( $P$ ,  $\nu_{\text{MAX}}$ ) and rotamer distributions ( $\chi$  and  $\gamma$ ) of the nucleoside analogues. It was shown that derivatives which are biased toward a “Northern” ( $3'$ -endo, N) sugar ring pucker were deaminated up to 65-fold faster and bound more tightly to the enzyme than those that preferred a “Southern” ( $2'$ -endo, S) conformation. This behavior, however, could be modulated by other structural factors. Similarly, purine riboside inhibitors of ADA that prefer the N hemisphere were more potent inhibitors than S analogues. These binding propensities were corroborated by detailed molecular modeling studies. Docking of both N- and S-type analogues into the ADA crystal structure coordinates showed that N-type substrates formed a stable complex with ADA, whereas for S-type substrates, it was necessary for the sugar pucker to adjust to a  $3'$ -endo (N-type) conformation to remain in the ADA substrate binding site. These data outline the intricate structural details for optimum binding in the catalytic cleft of ADA.

Adenosine deaminase (ADA,<sup>1</sup> EC 3.5.4.4) is an enzyme of the purine metabolic pathway that is crucial to mammalian immune system development (1). ADA catalyzes the conversion of Ado and dAdo (as well as other exogenous ligands) to their respective inosine derivatives plus ammonia, in a rapid and irreversible reaction (2, 3). Aberrations in the expression and function of ADA have been implicated in several disease states such as SCID, which is characterized by impaired B- and T-cell-based immunity resulting from an inherited deficiency in ADA (1, 4, 5). In contrast, highly elevated levels of ADA have been observed in malignant

human lymphocytes (6–8), making inhibitors of ADA important therapeutic targets for certain lymphomas and leukemias (9–11) such as HCL and CLL (12, 13). Consequently, the study of the structure, function, and kinetic properties of mammalian ADA has been an active area of research. An important advance in understanding the catalytic mechanism and substrate selectivity of this system has been the solution of several crystal structures of murine ADA in the presence of Ado analogues or inhibitors under various conditions (14–17). The most recent data (17) unequivocally established that the structures of the enzyme in complex with a transition-state analogue (dCF) and with a reaction coordinate analogue (HDPR) were very similar at pH 7.0 and that the complex structure with HDPR at pH 7.0 was nearly identical to that determined at pH 4.2 (14), where the enzyme is only 20% active (15). It was further determined that a  $\text{Zn}^{2+}$ -bound hydroxyl ion at the active site was the species responsible for the delivery of the ensuing inosine oxygen atom to the 6-position of the purine ring, thus confirming the catalytic requirement for zinc. In addition, hydrogen-bonding and hydrophobic interactions between amino acid side chains and relevant atoms of the nucleoside have been elucidated and correlated with previous site-directed mutagenesis studies (18, 19).

Most enzymes have strict conformational requirements for binding substrates or cofactors in structurally defined binding pockets. For nucleoside binding in general, and for ADA in particular, three well-defined conformational parameters are

\* Address correspondence to this author at the National Cancer Institute, National Institutes of Health, 37 Convent Dr., MSC4255, Bldg 37, Rm 5C02, Bethesda, MD 20892-4255. Phone 301-402-3113; FAX 301-402-2275; E-mail barchi@helix.nih.gov.

<sup>1</sup> Abbreviations: ADA, adenosine deaminase; Ado, adenosine; dAdo, 2'-deoxyadenosine; dCF, (8R)-hydroxyl-2'-deoxycoformycin; HDPR, (6S)-hydroxyl-1,6-dihydropurine ribonucleoside; DAA, 1-deazaadenosine; ddA, 2',3'-dideoxyadenosine; ara-A, arabinosyladenine;  $\alpha$ -FdA, 9-(2'-deoxy-2'-fluoro- $\beta$ -D-ribofuranosyl)adenine;  $\beta$ -FdA, 9-(2'-deoxy-2'-fluoro- $\beta$ -D-arabinofuranosyl)adenine;  $\alpha$ -FddA, 9-(2',3'-dideoxy-2'-fluoro- $\beta$ -D-erythro-pentofuranosyl)adenine;  $\beta$ -FddA, 9-(2',3'-dideoxy-2'-fluoro- $\beta$ -D-threo-pentofuranosyl)adenine;  $\alpha$ -FddP, 9-(2',3'-dideoxy-2'-fluoro- $\beta$ -D-erythro-pentofuranosyl)purine;  $\beta$ -FddP, 9-(2',3'-dideoxy-2'-fluoro- $\beta$ -D-threo-pentofuranosyl)purine; PR, purine riboside; 2'-dXA, 9-(2'-deoxy- $\beta$ -D-threo-pentofuranosyl)adenine; 6-Cl- $\alpha$ -FddP, 6-chloro-9-(2',3'-dideoxy-2'-fluoro- $\beta$ -D-erythro-pentofuranosyl)purine; 6-Cl- $\beta$ -FddP, 6-chloro-9-(2',3'-dideoxy-2'-fluoro- $\beta$ -D-threo-pentofuranosyl)purine; SAR, structure–activity relationships; NMR, nuclear magnetic resonance; HCL, hairy cell leukemia; CLL, chronic lymphocytic leukemia. SCID, severe combined immunodeficiency; PNP, purine nucleoside phosphorylase.

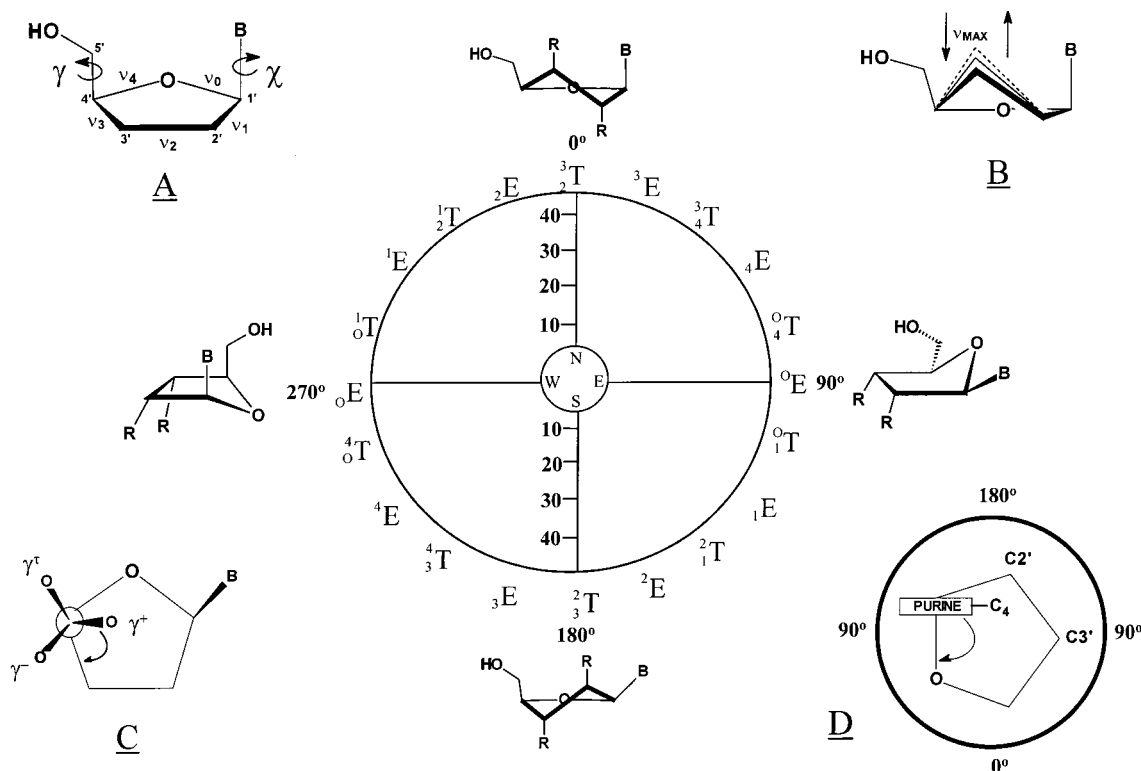
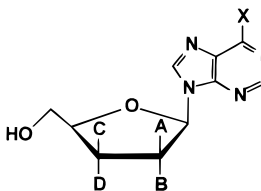


FIGURE 1: Pseudorotational cycle (center) illustrating the nucleoside ring pucker parameter  $P$  and description of other nucleoside structural parameters. A different twist or envelope form is obtained for every  $18^\circ$  torsion in the furanose ring angles from  $P = 0^\circ$  to  $360^\circ$ . (A) General view and labeling of ring torsion angles. (B) Description of maximum out-of-plane pucker parameter  $\nu_{\text{MAX}}$ . (C) Definition of angle  $\gamma$ . (D) Definition of angle  $\chi$  for a purine nucleoside.

crucial for determining whether an effective interaction with the protein will occur. These are (see Figure 1) (1) the angle about the N9–C1' glycosyl bond,  $\chi$ ; (2) the angle about the C4'–C5' bond,  $\gamma$ ; and (3) the sugar ring pucker, which is defined by the pseudorotational phase angle  $P$  and the degree of maximum ring pucker  $\nu_{\text{MAX}}$ . For the majority of nucleosides (20), the value of  $P$  normally falls within a narrow range of angles in the 3'-endo ("Northern", N) or 2'-endo ("Southern", S) hemispheres. The reports on the ADA complex crystal structures that have been solved to date describe the preferred disposition of the angles  $\chi$  and  $\gamma$  but offer only cursory references to the preferred N sugar ring conformation of the various adenosine analogues observed in the entire series of complex structures (14–17). The conformational attributes of the free substrates (in either solution or the solid state) are a result of the cooperative interplay of the nucleobase and the sugar moiety. The  $N \rightleftharpoons S$  equilibrium is consequently dictated by the balance of stereoelectronic gauche and anomeric effects, which are in turn dependent on the electronegativity, ionization state, steric bulk, and relative configuration of all the substituents on the sugar ring (21). Therefore, for efficient binding and catalysis, the substrate must present an appropriate balance of the above attributes. An earlier observation made in this laboratory, which was recently confirmed by the work of Meier et al. (22), showed that the conformationally N-biased nucleoside,  $\alpha$ -FddA (8, Table 1), was deaminated by ADA approximately 65 times faster than the S-biased  $\beta$ -FddA (7). On the basis of the X-ray data reported for the ADA complexes (vide supra), we reasoned that this difference may be due in part to the distinct preference to bind the N-biased  $\alpha$ -FddA (8) in the active site of ADA in place of the S-biased  $\beta$ -FddA

Table 1: Structures of Compounds Used in the Study

compound	abbreviation					
		A	B	C	D	X
1	Ado	H	OH	H	OH	NH <sub>2</sub>
2	dAdo	H	H	H	OH	NH <sub>2</sub>
3	ddA	H	H	H	H	NH <sub>2</sub>
4	ara-A	OH	H	H	OH	NH <sub>2</sub>
5	$\beta$ -FddA	F	H	H	OH	NH <sub>2</sub>
6	$\alpha$ -FddA	H	F	H	OH	NH <sub>2</sub>
7	$\beta$ -FddA	F	H	H	H	NH <sub>2</sub>
8	$\alpha$ -FddA	H	F	H	H	NH <sub>2</sub>
9	6-Cl- $\beta$ -FddA	F	H	H	H	Cl
10	6-Cl- $\alpha$ -FddP	H	F	H	H	Cl
11	PR	H	OH	H	OH	H
12	$\beta$ -FddP	F	H	H	H	H
13	$\alpha$ -FddP	H	F	H	H	H
14	2'-dXA	H	H	OH	H	NH <sub>2</sub>

(7). In this work, we have explored the binding of ADA with nucleoside substrate analogues in which the conformation of the sugar ring has been biased toward either the N-type or S-type pucker by virtue of the electronic character and stereochemistry of the groups at the 2' and 3' positions of the furanose ring (Table 1). We have determined the sugar ring conformations of these analogues in solution in an effort to account for their differential ADA activity using NMR spectroscopy and pseudorotational analysis. Kinetic studies and catalytic efficiencies experimentally confirmed that ADA

prefers sugars that favor the N-type pucker when compared to similar families of compounds favoring the S-type conformation. This trend holds unless specific structural factors prohibit a proper fit in the enzyme catalytic pocket. These data were confirmed by molecular dynamics simulations with several adenosine analogues docked into the active site of ADA. It was established that complexes with the analogues that favored and/or can easily adopt a N-type furanose pucker were lower in energy in an active-site model than those that favored an S-type ring pucker. This preference for a N-type conformation was further confirmed by the observation that some analogues whose sugar rings were biased toward S-type puckers in solution could adjust their conformations to an N-type pucker in the active-site model for effective binding to ADA.

## MATERIALS AND METHODS

**Chemicals and Synthesis.** ADA (calf intestine, EC 3.5.4.4) was purchased from Boehringer Mannheim (Indianapolis, IN). Ado (Table 1, **1**), dAdo (**2**), ddA (**3**), and PR (**11**) were obtained from Sigma Chemical Co. (St. Louis, MO). Ara-A (**4**) was purchased from Fluka Chemical (Ronkonkoma, NY), and  $\alpha$ -FdA (**6**) was obtained from R. I. Chemicals, Inc. (Orange, CA). The fluorinated nucleosides  $\beta$ -FdA (**5**),  $\beta$ -FddA (**7**), and  $\alpha$ -FddA (**8**) were synthesized previously (23). The 6-Cl- $\beta$ -FddA derivative **9** (24) and the  $\beta$ -FddP analogue **12** (25) have been reported and 6-Cl- $\alpha$ -FddA **10** was prepared by the methods described by Marquez et al. (23). The synthesis of **13** ( $\alpha$ -FddP) was performed in this laboratory and will be reported elsewhere. Compound **14** (2'-dXA) was prepared by the method of Hansske and Robins (26). dCF was obtained from the Drug Synthesis and Chemistry Branch, DTP, DCT, NCI. All other materials were purchased from Fisher Scientific (Pittsburgh, PA) or Aldrich Chemical Co. (Milwaukee, WI).

**Kinetic Analysis and Enzyme Assays.** Initial hydrolysis rates were determined by following the disappearance of substrate on a Shimadzu UV-PC 2101 spectrophotometer at 265 nm in 1 mL cuvettes with 0.1 M phosphate, pH 7.4 at 37 °C. A change in molar extinction coefficients for the deaminated products of  $\Delta\epsilon = -7900$  was assumed for all adenine analogues examined. For substrates with a  $K_M$  of 100  $\mu$ M or greater, high-performance liquid chromatography (vide infra) was used to follow the decrease in substrate concentration at 265 nm following the addition of ADA. At timed intervals, an aliquot was removed and the enzymatic hydrolysis was quenched by the addition of dCF (2  $\mu$ L, 0.5 mg/mL), a potent ADA inhibitor. The analyte (substrate) was separated and quantitated on a Beckman/Ultrasphere ODS 250  $\times$  4.6 mm column with a mobile phase of acetonitrile-water (15:85) with monitoring at 265 nm. Substrate concentrations in each kinetic assay were varied from 0.2 to 5 times the  $K_M$ , except for the 6-chloropurine analogues **9** and **10**, where the range was 0.2–2 times the  $K_M$  due to solubility limitations. A minimum of three determinations were made unless otherwise noted. Kinetic constants were determined by Lineweaver-Burk plots using Graph-Pad Prism V 2.01 (Graphpad Software, Inc. San Diego, CA), a personal computer-based curve-fitting program. Adenosine deaminase activity was measured spectrophotometrically by following the disappearance of adenosine at 265 nm in 1 mL cuvettes, at 25 °C, with 0.1 M phosphate, pH 7.4 (27). One unit is

defined as the amount of enzyme required to hydrolyze 1  $\mu$ mol of adenosine/min at 25 °C.

**Enzyme Inhibition Studies.** Inhibition constants were determined by monitoring the hydrolysis rates of adenosine (7–150  $\mu$ M) spectrophotometrically, as outlined above, in the presence of increasing concentrations of each inhibitor (compounds **11**–**13**) at pH 7.4, 37 °C. A minimum of three inhibitor concentrations were used for each determination. Double-reciprocal plots were used to determine the type of inhibition observed. The inhibition constants ( $K_i$ ) were determined from plotting the slopes of the reciprocal plots at each inhibitor concentration. The inhibitor concentration that reduces the rate of hydrolysis by 50% ( $IC_{50}$ ) was determined by following initial hydrolysis rates of adenosine (100  $\mu$ M) upon its addition to a solution of ADA (0.005 units/mL) preincubated for 10 min with varied concentrations of each inhibitor.

**NMR Spectroscopy.** NMR spectra were obtained at various temperatures on a Bruker AMX500 operating at 500 MHz for  $^1H$  with a triple resonance gradient probe (S/N on  $^1H \sim 650:1$ ).  $^{19}F$  spectra were acquired at 470.59 MHz with a dual selective  $^1H/^{19}F$  probe. Samples were dissolved either in  $D_2O$  or in  $D_2O$  buffered to pH 5.0 with  $CD_3COOD/NaOAc-d_3$ . Both  $^1H$ -coupled and broadband-decoupled  $^{19}F$  spectra were obtained to compare with simulated multiplets. One-dimensional  $^1H$  spectra used for coupling constant analysis were acquired with 64K data points and zero-filled to 128K with a sweep width of 5050 Hz and a relaxation delay of 2 s. Temperature control at 500 MHz was provided by a Eurotherm VT unit with fluctuations of no more than 0.1 K. Spectra were processed with resolution enhancement using Gaussian multiplication ( $lb = -1$ ,  $gb = 0.1$ ). For first-order resonances, coupling constants were read directly from the resolution-enhanced spectra, while more complex multiplets were analyzed by spectral simulation with HYPERNMR (Hypercube, Inc, Canada). Simulations of the eight spin systems were performed with the fluorine resonance set 100 ppm upfield of the nearest proton multiplet. Steady-state NOE difference spectra were obtained by use of the Bruker pulse sequence NOEMUL with the off-resonance spectrum acquired with the transmitter set within 100 Hz of the resonance being irradiated. Each transition of a resolved multiplet was spin-tickled for 40 cycles of 40–50 ms/multiplet, and transients were collected with a recycle delay of 5 s. Typical data sets included an average of 32 cycles of 8 scans/experiment.

**Ionization Constants.**  $pK_a$  values were measured by observing the change in chemical shift of the purine H8 proton as a function of pD by  $^1H$  NMR spectroscopy at 298 K. A total of 19 pD values were measured between pD 1 and 10. The sigmoidal curves from the plots of chemical shift vs pD were fit in an iterative least-squares manner with the program ORIGIN4.1 (Microcal Software Inc., Northampton, MA), and the  $pK_a$  was inferred from the inflection points and the first derivatives.

**Pseudorotational Analysis.** The ring conformations of the natural and synthetic nucleosides were analyzed with the program PSEUROT V.6.2 (29) (DOS version, purchased from Professor Cornelis Altona, University of Leiden, Leiden, The Netherlands) running on a Pentium II 333-MHz personal computer. This version includes an improved generalized Karplus equation for the iterative generation of



coupling constants based on the experimental data as described by Donders et al. (30). The standard values supplied with version 6.2 for substituent electronegativities were used in the iterations (1.37 for fluorine). The calculations were performed essentially as described earlier (31). Briefly, an iterative strategy was adopted whereby the pseudorotational parameters for each set of coupling constant data was calculated repeatedly after minor changes were systematically made in the starting parameters (see text and table legend for details). These data were examined to determine the best fit of the experimental and back-calculated coupling constants. RMS deviations of calculated and experimental values were generally  $<0.3$  Hz.

**Molecular Modeling.** Structure building and modeling were performed with QUANTA97 on a Silicon Graphics O2 workstation running the IRIX 6.3 operating system, using the CHARMm25 (MSI, San Diego, CA) force field. Models of both  $\alpha$ - and  $\beta$ -FddA (compounds **7** and **8**) were constructed with the 2D builder utility "Sketcher" contained in QUANTA. Conformational searches were performed with QUANTA-implemented tools. The coordinates used for docking were obtained from the ADA-transition-state inhibitor complex structure published by Wang and Quirocho (17) (PDB code 1A4M, 1998). The proteins were trimmed of all residues farther away than 14 Å from the active site. Atoms between 7 and 14 Å from the center of the active site were fixed in space to maintain the integrity of the model (the stability of these truncated enzyme structures was tested by performing minimizations and dynamic simulations in the presence of the bound HDPR ligand). The CHARMm25 parameter set was modified to include  $\text{Zn}^{2+}$ -associated parameters. Modifications were mainly based on parameters described previously (32) as well as on measurements from  $\text{Zn}^{2+}$ -containing complexes drawn from the Cambridge Structural Database. The charge on Zn was determined from ab initio molecular orbital calculations on a fully optimized ADA substructure using Gaussian94 (33) at the HF/6-31G\* level. The substructure contained Zn and its nearby residues. The calculated partial charge of +1.16 compared well with literature values (32). Molecular mechanics energy minimizations of the ligand-protein complexes were run employing the Adopted Basis Newton-Raphson (ABNR) algorithm. The nonbonded interactions cutoff was set to 14.0 Å, a shift function was used to smooth the transition for the van der Waals interactions, and a force switch function was used for the electrostatic interactions. The cutoff distance parameters used in the smoothing functions were CTOFNB = 12.0 Å and CTONNB = 8.0 Å, respectively. The complexes were not fully solvated since the ADA binding pocket is a deep cleft. However, specific water molecules on the surface of the catalytic site shown to be involved in interactions with the substrate in the solid-state complex structure (17) were maintained. Molecular dynamics simulations on the ADA-substrate complexes were performed with CHARMm25 on several DECAlpha CPU-based systems by heating to 300 K over 8 ps and equilibrating at 300 K for an additional 15 ps. Production dynamics simulations were performed for 250 ps with a step size of 0.001 ps at 300 K. Trajectories were recorded every 0.1 ps during the final 250 ps of the simulations. A shake algorithm was used to constrain covalent bonds to hydrogens to  $1 \times 10^{-8}$  Å. Force constants were subjectively assigned. The lowest energy frames were

Table 2: Kinetic Constants for Various Substrates of ADA<sup>a</sup>

compound	$K_M$ ( $\mu\text{M}$ )	$k_{\text{cat}}$ ( $\text{s}^{-1}$ )	$k_{\text{cat}}/K_M$ ( $\mu\text{M}^{-1} \text{s}^{-1}$ )
dAdo ( <b>2</b> )	$23.0 \pm 2.3$	245	10.6
$\alpha$ -FdA ( <b>6</b> )	$36.6 \pm 2.0$	283	7.4
Ado ( <b>1</b> )	$33.1 \pm 3.7$	188	5.7
$\alpha$ -FddA ( <b>8</b> )	$49.7 \pm 2.7$	259	5.2
$\beta$ -FdA ( <b>5</b> )	$50.2 \pm 5.8$	206	4.1
ddA ( <b>3</b> )	$85.1 \pm 4.1$	205	2.4
ara-A ( <b>4</b> )	$93.8 \pm 0.8$	46	0.49
$\beta$ -FddA ( <b>7</b> )	$330 \pm 19$	26.8	0.08
6-Cl- $\alpha$ -FddP ( <b>10</b> )	$5094 \pm 424$	29.1	0.006
6-Cl- $\beta$ -FddP ( <b>9</b> )	7500 <sup>b</sup>	3.0	0.0004

<sup>a</sup> Kinetic data were obtained spectrophotometrically at 37 °C by following the decrease in absorbance at 265 nm. For compounds with  $K_M$  above 100  $\mu\text{M}$ , HPLC analysis was used to monitor the changes in substrate concentration with time as described in Materials and Methods.

<sup>b</sup> Average of two experiments.

selected from the recorded trajectories and then minimized for 9000 steps, or until convergence, defined as energy gradient tolerance of  $\leq 0.001 \text{ kcal mol}^{-1} \text{ \AA}^{-1}$ . All binding energies were calculated with CHARMm25 using the full force field including van der Waals and electrostatic interactions with a dielectric constant set to 1.

## RESULTS

**Enzyme Hydrolysis and Kinetic Data.** On the basis of our original observation of the difference in deamination rates between  $\beta$ -FddA (**7**) and  $\alpha$ -FddA (**8**), we examined the influence of sugar conformation on ADA binding and catalysis for **7** and **8** and other paired sets of fluorine-containing substrates, such as  $\alpha$ -FdA (**6**) versus  $\beta$ -FdA (**5**) and 6-Cl- $\alpha$ -FddP (**10**) versus 6-Cl- $\beta$ -FddP (**9**). These data confirmed our initial observation that substrates favoring the N-conformation (see NMR section) were deaminated faster ( $k_{\text{cat}}$ ) and more efficiently ( $k_{\text{cat}}/K_M$ ) than substrates favoring the S conformation. The kinetic data for the synthetic adenine-containing nucleoside analogues are shown in Table 2. The Michaelis binding constants ( $K_M$ ) shown cover a 300-fold range with catalytic efficiencies ( $k_{\text{cat}}/K_M$ ) spanning a range of  $\sim 3 \times 10^4$ -fold. The data obtained for the F-containing analogues prompted us to examine whether the preferred pseudorotational parameter  $P$  for various substrates in solution, including the natural substrates, Ado (**1**) and dAdo (**2**), correlated with the rate and efficiency of the deamination reaction. The data for **1** and **2** showed that removal of the 2'-hydroxyl group enhances slightly both ADA binding ( $K_M$ ) and turnover rate ( $k_{\text{cat}}$ ). The findings for ddA (**3**), where both the 2'- and 3'-hydroxyl groups have been removed, however, resulted in a substrate that did not bind as tightly but was catalyzed ( $k_{\text{cat}}$ ) as efficiently as adenosine and somewhat less efficiently than dAdo. A similar trend can be shown in the corresponding fluorinated series. When the 3'-hydroxyl group is present, the analogues ( $\alpha$ -FdA, **6**, and  $\beta$ -FdA, **5**) were better substrates and were more readily hydrolyzed (lower  $K_M$  and higher  $k_{\text{cat}}$ ) than the corresponding dideoxy analogues,  $\alpha$ -FddA (**8**) and  $\beta$ -FddA (**7**), respectively. With the exception of ara-A (**4**), the only compound examined with an ara arrangement of the furanose hydroxyl groups, and  $\beta$ -FddA (**7**), the rest of the analogues (**1**–**3**, **5**, **6**, and **8**) were shown to be good substrates with reasonably close kinetic parameters. With compounds **4** and **7**, significant differences of ca. 10-fold relative to the better substrates began to emerge.

Table 3: Inhibition Constants for ADA with Purine Nucleoside Analogues<sup>a</sup>

compound	$K_i$ ( $\mu$ M)	$IC_{50}$ ( $\mu$ M)	inhibition type
PR ( <b>11</b> )	10.7	46.4	competitive
$\alpha$ -FddP ( <b>13</b> )	20	125	competitive
$\beta$ -FddP ( <b>12</b> )	ND	>400	ND

<sup>a</sup> Inhibitors were preincubated at 37 °C with ADA for 10 min before the addition of substrate. Initial reaction velocities were fitted to Michaelis–Menten double-reciprocal plots and  $K_i$ s were calculated as described in Materials and Methods.

Table 4: Structural Parameters for Adenosine Analogues<sup>a</sup>

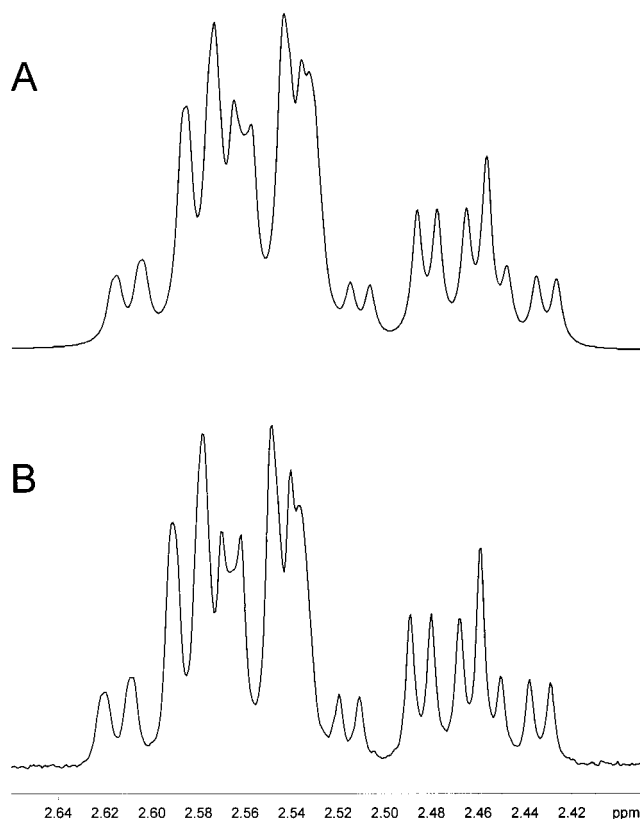
compound	$\gamma^+$ (%)	$\gamma^t$ (%)	$P_N$	$\nu_N$	$P_S$	$\nu_S$	RMS	% $N$
Ado ( <b>1</b> )	64	24	10.9	39.0 <sup>b</sup>	153.3	28.5	0.092	27
dAdo ( <b>2</b> )	59	30	9.0 <sup>b</sup>	36.0 <sup>b</sup>	155.0	31.6	0.155	28
ara-A ( <b>4</b> )	56	37	−1.3	36.0 <sup>b</sup>	140.2	36.0 <sup>b</sup>	0.081	76
$\beta$ -FdA ( <b>5</b> )	42	45	9.0 <sup>b</sup>	36.0 <sup>b</sup>	131.9	37.0	0.038	36
$\alpha$ -FdA ( <b>6</b> )	73	27	−5.0	38.0 <sup>b</sup>	119.2	38.0 <sup>b</sup>	0.035	76
$\beta$ -FddA ( <b>7</b> )	38	52	−10.0 <sup>b</sup>	36.0 <sup>b</sup>	132.7	38.1	0.361	19
$\alpha$ -FddA ( <b>8</b> )	62	34	−0.2	35.9	160.0 <sup>b</sup>	36.0 <sup>b</sup>	0.126	99

<sup>a</sup> NMR coupling constants were collected between temperatures of 278 and 353 K in D<sub>2</sub>O buffered to pH 5.0 with HOAc-*d*<sub>4</sub> and NaOAc-*d*<sub>3</sub>. Pseudorotational analysis was performed with PSEUROT 6.2 and an iterative approach was used. Initially, all parameters to be determined [ $P_N$ ,  $P_S$ ,  $\nu_{MAX}(S)$ ,  $\nu_{MAX}(N)$ , and  $X_S$ ] were allowed to refine and further runs either held one or both  $\nu_{MAX}$  values constant or held the  $P$  and  $\nu_{MAX}$  values of the alleged minor isomer constant.  $\nu_{MAX}$  values were varied in increments of 1° between 34° and 44° and holding  $P$  constant from −36.0° to 36.0° in 9.0° increments and from 140° to 200° in 15° increments for  $P_N$  and  $P_S$ , respectively. <sup>b</sup> Values held constant during calculations.

ADA shows improved catalytic efficiency and binding for the 2'- $\alpha$ -fluorinated sugar analogues **6** and **8** over their respective 2'- $\beta$ -fluorinated analogues **5** and **7**. This trend holds for all paired fluorinated compounds, including the 6-chloropurine analogues **9** and **10**, which are among the poorest ADA substrates in our panel, with  $K_M$  values in the low millimolar range. This poor binding probably reflects the loss of important contacts (H-bonding) by replacing the amino group with chlorine at the active site. Additionally, the electronic effect of the chlorine atom may lower the hydration capacity of the 6-position of the purine system.

**Inhibition Studies.**  $K_i$  values of compounds **11**–**13** are shown in Table 3. The fluorinated derivatives of 2',3'-dideoxypurine (**12** and **13**) were compared with the known inhibitor purine riboside (**11**). Both **11** and **13** were found to be competitive inhibitors of ADA with the  $\alpha$ -FddP analogue **13** being a comparable inhibitor to the purine riboside **11**. In contrast,  $\beta$ -FddP (**12**) was the poorest inhibitor of the three compounds studied with an  $IC_{50}$  above 0.4 mM. This trend parallels what was described above, i.e., nucleosides with an  $\alpha$ -F substituent at C2' interact with the ADA active site more efficiently than those containing a C2'  $\beta$ -fluorine atom.

**NMR Spectroscopy and Pseudorotational Analysis.** To examine the structural features that may correlate with the observed kinetic data, one-dimensional <sup>1</sup>H spectra were collected at various temperatures for compounds **1**, **2**, **4**, and **5**–**8**. Table 4 lists the structural parameters calculated from the coupling constant data derived from these spectra. Temperature-dependent changes in the coupling constants were examined for all eight analogues between 278 and 353

FIGURE 2: Simulated (A) and experimental (B) 3',3'' region of the spectrum for compound **8**.

K (the details of the full coupling constant and <sup>19</sup>F NMR analysis of the analogues will be published elsewhere). These changes were used to calculate the pseudorotational parameters  $P$  and  $\nu_{MAX}$  with the program PSEUROT (vide infra). The majority of the couplings could be read directly from the resolution-enhanced 1D spectra, but multiplets displaying second-order distortions were simulated. An example of this is shown in Figure 2, which shows the quality of the simulation for the overlapping 3',3'' protons of compound **8**. The H4'–H5' and H4'–H5'' coupling constants were used to calculate the preferred rotamer distribution ( $\gamma^+$ ,  $\gamma^t$ ,  $\gamma^-$ ) about the C4'–C5' bond according to Haasnoot et al. (34) (see Figure 1). In addition, one-dimensional steady-state NOE difference spectra were recorded for the fluorinated analogues to obtain a qualitative measure of the glycosyl torsion angle  $\chi$  (35). The pseudorotational parameters in Table 4 were calculated with the program PSEUROT 6.2 employing updated values for the substituent electronegativity constants. The program assumes a dynamic N/S equilibrium for the nucleoside furanose ring and derives the mole fraction of the ring pucker populating each hemisphere of the pseudorotational cycle (see Figure 1). An iterative approach was taken where different parameters to be determined ( $P_N$ ,  $P_S$ ,  $\nu_N$ ,  $\nu_S$ ) are held fixed or set to be refined. If there is reason to believe a specific furanose derivative may prefer a particular ring pucker (N or S), the minor conformer is normally held fixed during the iteration. The details of the calculations are described in the legend to Table 4. The quality of the data is measured in the RMS deviation of the calculated and experimental coupling constants. In general, these errors were less than 0.3 Hz, indicating the parametrization of the program is well suited to the input data. The

exception was compound **7**, which showed RMS deviations of 0.3–0.4 Hz, similar to results obtained previously on the equivalent F-containing pyrimidine dideoxynucleosides (25). The combination of these data gave an overall picture of the nucleoside conformation in solution.

Detailed NMR measurements for **1** and **2** have been carried out previously in D<sub>2</sub>O (36) and at various pD values (37), but they were repeated here in pD 5.0 buffer to independently confirm the population differences observed. The data obtained were similar to those calculated by Plavec et al. (36), where both **1** and **2** prefer the S hemisphere in solution by as much as 72% at 298 K. Compound **4** (ara-A) has been studied by X-ray crystallography (38) and NMR spectroscopy (39), but a calculation of the actual pseudorotational parameters using PSEUROT was not available. The crystal structure of compound **4** shows a distinct N pucker (38), and the pseudorotational analysis described here confirms that this conformation is also highly populated in solution (Table 4). This result is probably counterintuitive when one considers that the combined gauche effects (40, 41) of O4'–C1'–C2'–O2'' and O4'–C4'–C3'–O3' in the ara configuration should favor a 2'-endo/3'-exo (S) arrangement; however, the inversion of configuration at C2' causes the O3'–C3'–C2'–O2' and O2'–C2'–C1'–N9 gauche effects to drive the conformation of the sugar to the opposite 3'-endo/2'-exo (N) conformation. These forces will add to the anomeric effect, which normally drives the sugar conformation to the N (42). In solution, therefore, as in the crystal structure, the conformation of ara-A remains N, a fact that argues in favor of the strength of the O2–C2'–C1'–N9 gauche effect, which on geometric grounds should be decisively stronger than the same gauche effect in a ribo configuration by facilitating a more favorable  $\sigma \rightarrow \sigma^*$  orbital mixing (21).

For the fluorinated analogues (**5**–**8**) we found that, in general, the fluorine gauche effect predominates over both the oxygen gauche effect and, at times, the anomeric effect (42) in driving the pseudorotational equilibrium. Analogues with a 2'- "up"-oriented fluorine are biased to the S whereas those with a 2'- "down" disposition of the fluorine atom are N-puckered. Compounds **5**–**8** are close to "normal" ranges of N (**6** and **8**) and S (**5** and **7**) puckers (by definition, an N conformation has a *P* value of  $0^\circ \pm \sim 18^\circ$  and the value for the S pucker is in the  $180^\circ \pm \sim 18^\circ$  range). The best fit of the data resulted in a *P* value of near  $130^\circ$  for both compounds **5** and **7**, which translates to an approximate C1'-exo envelope conformation (Figure 1) with 64% and 81%, respectively, of the ring pucker in the S hemisphere at 25 °C. Both N-disposed compounds, **6** and **8**, had calculated *P* values for the most abundant conformers (76% and 99%, respectively) close to  $0^\circ$ , which defines a "true" N conformation (C3'-endo, C2'-exo twist, Figure 1). These results confirm that the fluorine gauche effect is dominant over other stereoelectronic factors in these compounds, not unlike what was shown previously for other furanose-monofluorinated nucleoside analogues (31, 43).

A stiffer sugar pucker also influences the orientation of the 5'-hydroxyl group (angle  $\gamma$ ) in the fluorinated analogues. Compounds in the S hemisphere (**5** and **7**) prefer the  $\gamma^+$  rotamer slightly over  $\gamma^+$  (20) (see Figure 1), but the compounds in the N hemisphere (**6** and **8**) prefer the  $\gamma^+$  rotamer. The  $\gamma^+$  rotamer was observed in the recent crystal

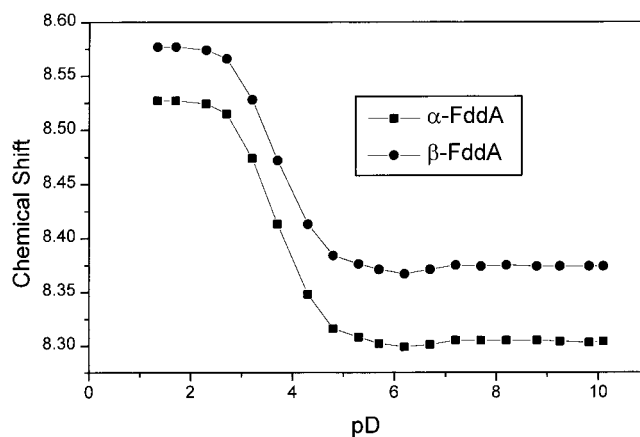


FIGURE 3: pD vs chemical shift curves for the H8 proton of  $\beta$ -FddA (**7**) and  $\alpha$ -FddA (**8**). The  $pK_a$  values were obtained from the inflection points after the curves were fitted to a sigmoidal distribution equation.

structures of ADA with different inhibitors (14–17). Therefore, a strong preference for a specific C4'–C5' rotamer may influence the binding and catalytic efficiency of synthetic analogues of adenosine.

NOE analysis suggested that the disposition of the purine ring (angle  $\chi$ ) was predominantly in the anti range for all of the fluorinated analogues, with a small proportion of the syn disposition observable for  $\alpha$ -Fda **6** and  $\alpha$ -FddA **8** (data not shown). The percentages of the enhancements between H8 and H1' coupled with the presence of NOEs of H8 with the protons occupying *endo* positions on the sugar ring supported these conclusions (35). Since ADA binds substrates with the base rotated in the anti position, as evidenced by the recent crystal structure data (14–17), small populations of the syn rotamer may be detrimental to substrate efficiency.

**Ionization Constants.** Literature values of 3.65 and 3.40 for the  $pK_a$  of Ado (**1**) have been determined previously by spectrometry (44) and electrophoresis (45), respectively. These values are in good agreement with the ionization constants of compounds **7** and **8** determined by us using NMR spectroscopy. Figure 3 shows the change in chemical shift of the H8 proton of compounds **7** and **8** with pD. The fluorine atom, whether in the 2'- $\alpha$  or 2'- $\beta$  conformation on the sugar, appears to have minimal influence on protonation of the purine ring since the  $pK_a$  values for **7** and **8** derived from the inflection points of these curves were 3.68 and 3.67, respectively.

**Molecular Modeling.** Selected compounds were docked into the crystal structure of ADA and their behavior during molecular dynamics simulations was examined. Along with the natural substrate dAdo (**2**) and the well-known antiviral agent ara-A (**4**), we used the pair of 2',3'-dideoxy-2'-fluoroadenosines (**7** and **8**) to compare the effect of the stereochemistry of the fluorine atom on the stability of the model complexes. Compound **2** was included in the modeling because we wanted to explore the flexibility of this natural ADA substrate, which shows the highest catalytic efficiency when compared to the synthetic analogues. To this end, several runs were made where the starting *P* values for **2** were close to the solution conformation (S, *vide supra*) although the crystal structure of **2** is in the N conformation (46). Compound **4** was examined as an example of a substrate that prefers a N ring pucker in both the solid and



Table 5: Starting and Final Parameters for Compounds Used in ADA Docking Studies

structural parameter	initial and final values <sup>a</sup>						
	$\beta_x$ (7)	$\beta_i$ (7)	$\beta_{xp}$ (7)	$\alpha_i$ (8)	$\alpha_{ig}$ (8)	dAdo (2)	Ara-A (4)
$\gamma_{\text{initial}}$	-177.4	56.1	-177.4	56.1	-177.4	-177.4	178.9
$\gamma_{\text{final}}$	71.2	66.8	178.4	70.1	66.7	68.2	164.8
$\chi_{\text{initial}}$	-92.7	-111	-92.7	-111.2	-125.8	-92.7	-108.4
$\chi_{\text{final}}$	-123.5	-111.8	-97.3	-117.8	-122.2	-123.3	-98.1
$P_{\text{initial}}$	184.2	129.2	184.2	19.1	19.1	184.2	26.2
$P_{\text{final}}$	36.8	43.2	183.2	36.0	43.2	37.8	168.3

protein residue	atom on nucleoside	relevant distances of substrate atoms to protein atoms <sup>b</sup> (Å)						
		$\beta_x$ (7)	$\beta_i$ (7)	$\beta_{xp}$ (7)	$\alpha_i$ (8)	$\alpha_{ig}$ (8)	dAdo (2)	Ara-A (4)
Asp-19 OD1	5'-OH	2.1	2.1	4.3	2.0	2.0	2.0	4.4
Asp-19 OD2	5'-OH	1.9	2.0	5.0	1.9	2.0	1.9	4.8
Asp-19 OD2	2'-OH							2.3
Asp-296 HD2	N7	2.2	2.1	2.2	2.2	2.0	2.2	2.2
Cys-353 SG	5'-OH			2.5				2.9
Glu-217 OE1	N1-H	1.9	2.0	1.9	2.0	2.0	1.9	2.0
Glu-217 OE2	N1-H	2.3	2.0	2.4	2.0	2.7	2.3	3.3
Gly-184 H	N3	2.2	2.2	2.2	2.2	2.2	2.3	2.2
His-17 HD1	5'-O	1.8	1.8	1.9	1.8	1.8	1.8	1.9
His-238 HE2	6-O	2.4	2.1	2.4	2.3	2.3	2.4	2.2
H <sub>2</sub> O (2357) <sup>c</sup>	3'-OH						2.2	
H <sub>2</sub> O (2362) <sup>c</sup>	3'-OH							2.3

<sup>a</sup> The values marked initial are those used before docking and simulations, and the values marked final are those after molecular dynamic simulations in the presence of the protein. Description of each conformer is explained in the text. <sup>b</sup> Values shown are those obtained after dynamic simulations of the docked complexes with the conformers labeled in the top half of the column. Protein residue numbers correspond to the labels given in ref 17. <sup>c</sup> H<sub>2</sub>O refers to the O atom of a particular crystal water molecule in the vicinity of the nucleoside atom.

solution states, and yet it is a less efficient substrate than compounds **1–3**, **5**, **6**, and **8** and comparable to **7** (Table 2). Table 5 lists the starting and final values of particular structural parameters (values for  $P$ ,  $\gamma$ , and  $\chi$  before and after the dynamics simulations) along with the distances from relevant atoms on the substrate to specific protein residues for the several conformers used in the docking and molecular dynamics simulations. Where available, we used the crystal structure coordinates of the ligands to be docked into ADA. Crystal structures were used for compounds **4** (38) and **7** (47). Conformations for **8** were obtained as described below.

To initially explore the conformational space available to the fluorinated analogues within the context of CHARMm25, compounds **7** and **8** were subjected to an exhaustive conformational search. It was found that most of the sugar ring puckers for **7** and **8** calculated from this search were predominantly of the S and N types, respectively, demonstrating a qualitative agreement of the molecular mechanics force field calculations with the NMR and pseudorotational data. The  $P$  values of the most highly populated conformers generated in the conformational search were used to construct models of compounds **7** and **8** for the docking studies with ADA. Since the calculations of the  $\gamma$  and  $\chi$  angles from NMR data have higher error margins than crystallographic measurements, we employed the experimental coordinates from the crystal structure of **7** (47) along with information from the HDPR coordinates within the ADA active site (17) to complete the assembly of the starting conformations to be modeled in the ADA active site for **7** and **8**. The crystal structure coordinates from Bunick and Voet (38) were used for compound **4** since they were similar to the solution conformation determined in this study.

For  $\beta$ - and  $\alpha$ -FddA (**7** and **8**), five conformers (three for **7** and two for **8**) were used and are designated  $\beta_x$ ,  $\beta_i$ ,  $\beta_{xp}$ ,  $\alpha_i$ , and  $\alpha_{ig}$ , respectively. The  $\beta_x$  conformer represents the

X-ray coordinates of **7** from (47), whereas  $\beta_{xp}$  is similar to  $\beta_x$  with the exception that the  $P$  value calculated from the crystal structure (184.2°) was held fixed during the dynamics simulations.  $\beta_i$  and  $\alpha_i$  (for **7** and **8**, respectively) were obtained by applying the optimum  $P$  value from the conformational search procedure and rotating the  $\chi$  and  $\gamma$  angles to -111° and 56.1°, respectively, which are in the range we refer to as “ideal”, or closest to the average of the values obtained from the ligands in the various ADA crystal structures.  $\alpha_{ig}$  is similar to  $\alpha_i$  with the exception that the initial  $\gamma$  angle was set to the same value as in  $\beta_x$ . The conformers were docked into the ADA-HDPR active site and the ensuing complexes were subjected to energy minimization and molecular dynamics simulations according to the protocol outlined in Materials and Methods.

The complexes of compound **8** and ADA were stable throughout the simulations and the sugar pucker remained in the N hemisphere. However, when the conformers of **7** ( $\beta$ -FddA), which all started with an S pucker, were docked and minimized, the sugar adjusted toward the N range. For example, in the ADA- $\beta_x$  complex, the initial  $P$  value of 184° (pure S) adjusted to 165° upon simple minimization. During the dynamics simulations, the  $\beta_x$  conformer completely flipped to a N conformer with a  $P$  value of 36.8° (Figure 4a). The  $\gamma$  angle adjusted from the starting value of -177.4° ( $\gamma^+$  range) to 71.2° ( $\gamma^+$  range). If the ring pucker of **7** was constrained in the S hemisphere ( $\beta_{xp}$  conformer) and the dynamic simulation repeated, the  $\gamma$  angle does not adjust to the “proper”  $\gamma^+$  range and hence the critical protein–ligand interactions of the CH<sub>2</sub>OH- group remain disrupted in this complex (Figure 4b). For conformer  $\beta_i$  (initially  $\gamma^+$  for the C4'–C5' torsion and a  $P$  value in the S hemisphere), the angle  $\gamma$  retains an “ideal” value during the dynamics simulation while the ring pucker adjusts to a N-type pucker (data not shown). These results show that, regardless of the

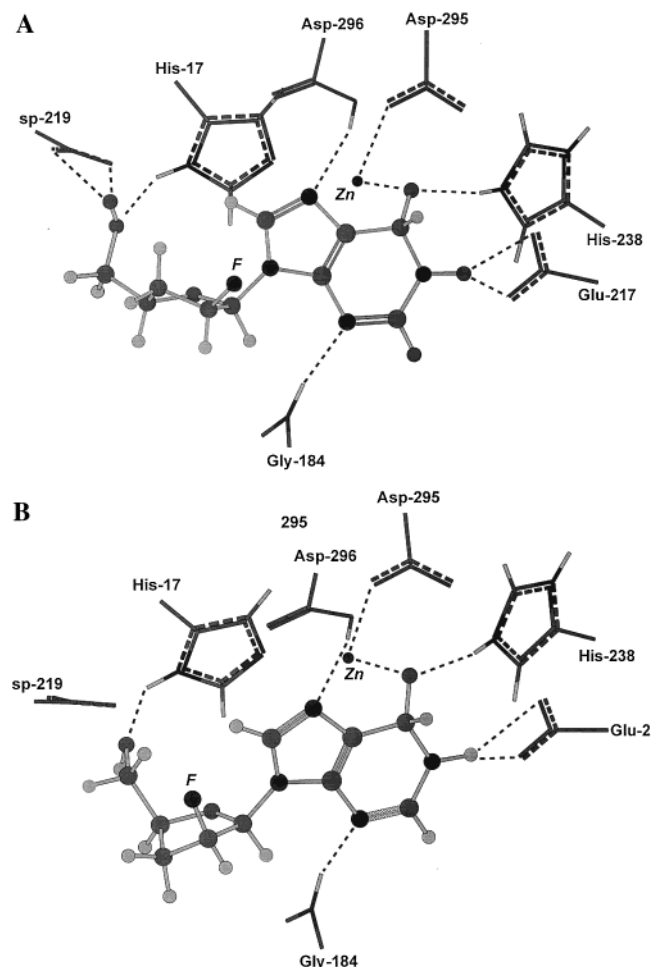


FIGURE 4: (A) ADA active-site model of the complex with compound **7** where all degrees of freedom were allowed to adjust. (B) ADA active-site model of the complex with compound **7** where the ring pucker was held constant in the S hemisphere. The fluorine atom is labeled (F).

initial conformation of **7**, the furanose ring will adjust to a N conformation after dynamics simulations in the ADA active site.

Similar results were obtained for the ADA/dAdo (**2**) complexes. During one particular simulation, simple minimization adjusted the pseudorotational parameter from  $P = 184.2$  to  $P = 83.2$ , and during the dynamics run  $P$  was reduced to 46.7. As mentioned above, the starting conformation for **2** is predominantly S in solution as calculated from PSEUROT. It took much less energy ( $\sim 1$  kcal/mol) for **2** to flip to N than for **7** (3.7 kcal/mol), indicating the enhanced flexibility of the sugar ring of **2** relative to **7** in the ADA active site.

The results obtained when compound **4** was modeled in the ADA active site were more unexpected. Being an N sugar, it was anticipated that the initial ring pucker would be stable at the active site. However, after dynamics simulations, the ara-A sugar ring had adjusted to an S conformer. The C4'–C5' rotamer, initially in the  $\gamma^t$  range, did not change during the calculations. A close examination of the protein residues around the substrate revealed that, when the 2'-OH is "up" in the pseudoequatorial position (N-conformer), a serious steric clash with hydrophobic residues ensued, in particular with a methyl group of Leu62. This caused the sugar ring to flip to the less desirable S

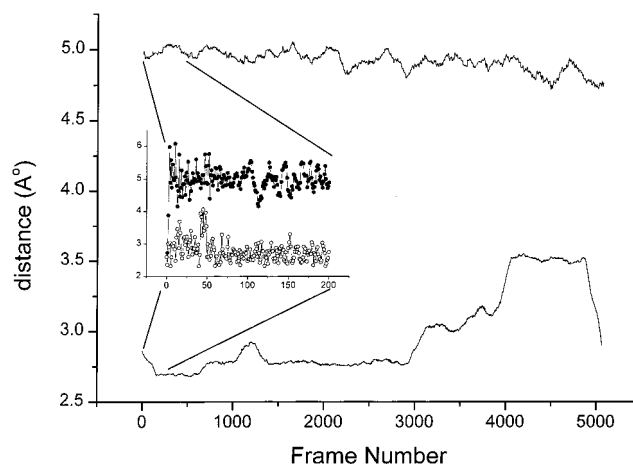


FIGURE 5: Graph of the distance between O2' of compound **4** and a Leu62 methyl (side-chain) proton. Dynamics simulations were run for a total of 250 ps and 5000 frames were collected. Note that the curves are strongly smoothed (to show the overall trend) using averaging with a sliding window with a 200-data point width. The inset is the expanded, unsmoothed section of the first 200 frames illustrating the flip from the starting N conformer to a S conformer to relieve the steric clash with the protein (●). The plot with open circles is derived from a dynamics simulation where the sugar pucker was held fixed and the O2'–Leu62 methyl distance remains within van der Waals contact distance.

hemisphere with a pseudoaxial arrangement of the hydroxyl groups at both the 2'- and 3' carbons to relieve this close contact. Figure 5 depicts the distance between the O2' atom and a close side-chain hydrogen atom of a methyl group of Leu62 from ADA. If the ring pucker is constrained, the distance remains approximately the same (around 2.7 Å) for most of the simulation and hence the free energy of the complex remains high. If the ring pucker is allowed to adjust, the distance rapidly jumps from an initial value of 2.5 to 6 Å and remains there throughout the simulation. The inset in Figure 5, with unsmoothed curves and much greater temporal resolution, nicely shows the (normal) dynamical fluctuations for the unconstrained case (●), whereas for the constrained ring pucker, one clearly sees a lower threshold of about 2.2 Å where the steric clash of the aforementioned atoms begins (○).

## DISCUSSION

ADA is present in almost all tissues, but a particularly large concentration of this enzyme is found in cells of lymphoid origin. A primary function of ADA in T- and B-cell populations is the catabolism of Ado, dAdo, and analogues to inosine derivatives, which are substrates for phosphorolysis by PNP. The resulting hypoxanthine is further processed to uric acid by xanthine oxidase. This is a major detoxification mechanism in lymphoid tissue, thus eliminating excess dAdo. Via its triphosphate, dAdo inhibits DNA synthesis and leads to apoptotic cell death and a depletion of the T- and B-cell population leading to immunodeficiency (1, 4, 5), a characteristic of patients with SCID who lack appropriate levels of ADA. In contrast, elevated levels of ADA have been found in the tissue from several leukemias, which suggested that targeted disruption of ADA activity could be an effective therapy against such tumors. Research regarding the structure and function of ADA has led to the discovery of novel therapeutics which are in clinical use for the treatment of such cancers (12, 13, 48, 49).



**Analogue Structures.** Perhaps the single most important advance in the “rational” design of tight binders and inhibitors of ADA (or any other enzyme system) is the availability of molecular coordinates of the receptor or receptor–substrate(inhibitor) complexes. A clear understanding of the structural requirements for substrate binding allow for appropriate modifications to be designed into synthetic analogues. In this work, we have studied the ADA SAR of nucleoside congeners whose structural features (Figure 1) are controlled by a judicious choice of functionality on the sugar ring. It has been well established that the furanose ring pucker of a nucleoside is influenced by a variety of factors including the nature and electronegativity of the ring substituents, steric bulk, and the anomeric effect. The influence of substituent electronegativity on ring pucker is manifested in the gauche effect, which results from the tendency of electronegative groups on vicinal carbon atoms to assume a gauche relationship (21, 40, 41). In ribonucleosides, several gauche effects are operable at the same time ( $O4'-C1'-C2'-O2'$ ,  $O4'-C4'-C3'-O3'$ ,  $O3'-C3'-C2'-O2'$ , and  $O2'-C2'-C1'-N$ ), whereas in 2'-deoxynucleosides the situation is simplified to the lone  $O4'-C4'-C3'-O3'$  torsion angle, which prefers a gauche disposition. The replacement of oxygen with other electronegative groups can maintain, enhance, or reduce these effects (36, 37, 50–53). Owing to its unsurpassed electronegativity, the introduction of a fluorine (F) atom to the 2'- or 3'-position normally imparts a distinct bias to the furanose sugar ring pucker. The anomeric effect, which acts either in concert with or against the gauche effect, tends to drive the pseudorotational equilibrium toward the N (50–53). The following briefly describes some of the individual cases as to their NMR-derived N/S disposition.

Herein we have shown that the F-gauche effect drives the pseudorotational equilibrium of compounds **5–8**. The F-gauche effect is capable of “overriding” the effect of other electronegative groups, but there is still a balanced interplay between the distinct forces around the sugar ring. For example, in the 2',3'-dideoxy cases (**7** and **8**) the two operational effects are the  $O4'-C1'-C2'-F$  gauche effect and the anomeric effect. Compound **8**, with a “down” F atom, is virtually 100% N at 25 °C due to the additive anomeric and gauche effects driving the ring pucker to the N (Table 4). Alternatively, the gauche effect of compound **7**, with an “up” F atom, opposes the weaker anomeric effect (50–53), causing the equilibrium to favor the S conformation but with a ~4/1 S/N ratio at 25 °C. Although we did not perform a detailed PSEUROT analysis on diastereomeric pairs **9**, **10** and **12**, **13**, a cursory examination of the NMR data suggested that the trend outlined above is obeyed, where a 2'-F atom in the “up” position dictates a preference for the S conformer and a 2'-F atom in the “down” position drives the equilibrium to the N.

The situation is more complex for **5** and **6** due to the competing electronic effects of the 3'-OH group. Compound **6** prefers the N, probably due to the same gauche and anomeric effects functional in **8**, which tend to surpass the  $O4'-C4'-C3'-O3'$  gauche effect. The calculated pseudorotational parameters also vary from those derived for **8** (Table 4) but remain in the N hemisphere. Interestingly, compound **5** occupies a conformation with very similar pseudorotational parameters as those calculated for the

dideoxy analogue **7**. The ring pucker, being close to a C1'-*exo* envelope, positions the F and 3'-OH groups in a gauche orientation but also (nearly) eclipses these groups with the adjacent hydrogen atoms. PSEUROT calculations using the coupling constants observed for **5** gave excellent RMS deviations from experimental values (<0.1 Hz), which were much lower than those for the dideoxy compound **7**. In the case of **7**, this may result from nonoptimum parametrization of the PSEUROT program for this type of ring system. A complete study of the structural parameters for compounds **5–8** using a modification of the PSEUROT program is the subject of a separate paper.

Steady-state 1D NOE data offers a qualitative picture of the preferred rotation about the glycosyl bond (35, 54). There were no strong interactions observed between H8 and H1' typical for the base in the syn orientation (data not shown). Interestingly, both **6** and **8**, which are biased toward the N hemisphere, showed weak correlations between H8 and H1', whereas these peaks were virtually absent in the S-disposed compounds **5** and **7**. This is contrary to what is observed in crystal structures of a series of nucleosides, which show that syn  $\chi$  angles are generally associated with C2'-*endo* (S) puckers (20, 55). Since it is well established that substrates and/or inhibitors of ADA bind in an anti conformation, we assume that although there may be a small proportion of the syn rotamer populated in some analogues, flexibility in solution allows proper orientation of the  $\chi$  rotamer in compounds **5–8** to easily adjust to the appropriate anti conformation.

**ADA Binding and Catalysis: Optimal Structural Features?** The data in Table 2 detail the binding capacity and the catalytic efficiency of the analogues tested. It was clearly established that for pairs of compounds whose sugar rings pucker in opposite hemispheres on the pseudorotational cycle, the N compounds are always superior in binding and substrate efficiency. However, there emerged a pattern of other factors that play supportive or destructive roles in the interaction of these compounds with ADA. These are discussed below.

Table 2 is organized in order of catalytic efficiency defined as the turnover number,  $k_{cat}$ , divided by the binding constant,  $K_M$  (micromolar). ADA has evolved to where this performance has been optimized for dAdo, undoubtedly due to the importance of dAdo catabolism in vivo (vide supra). Yet, in terms of absolute hydrolysis rate ( $V_{MAX}$ , not shown) or turnover number ( $k_{cat}$ ), the two F-containing synthetic analogues (**6** and **8**) were superior. Both of these compounds are heavily biased toward the N conformation. The binding constant for Ado (**1**) is favorable but the reaction rate is inferior to the N compounds or the flexible dAdo (**2**). Compounds **5** and **3** are nearly equal in reaction rate but differ in binding efficiency. Arabinosyladenosine (ara-A, **4**) reacted slower than compound **5**, even though it predominantly populates the N pucker in solution. The interplay of ring pucker and the position of the 2'-hydroxyl group probably combine to render this conformation incompatible with the active site as we have seen in our modeling studies. The 2',3'-dideoxyadenosine analogue **3**, although puckered in the N conformation, is nearly equivalent to the natural substrates.

The weakest substrate of the adenine-containing analogues was  $\beta$ -FddA (**7**), a compound that highly favors a S

conformation. The 6-chloro derivatives **9** and **10** were also very poor substrates perhaps due to the loss of H-bond donation from the amino group to the critical zinc atom in the active site. The chloro group at position 6 may also influence the hydration capacity of the purine ring. However, these compounds still followed the general trend where the N analogue (**10**) displayed a catalytic efficiency about 15 times that of the S analogue (**9**). This tendency also held for the purine-based inhibitors **12** and **13** (Table 3). From this varied data set, we can conclude that N compounds are superior to S compounds in both binding to ADA and turnover rate. In addition, analogues that pucker in the S and contain a 3'-ribo hydroxyl group are more efficient than those deoxygenated at C3' (compare **5** and **7**). Flexibility is also a strong determinant in catalytic efficiency, since the natural substrates must invert their ring puckers to accommodate the active site.

The picture is certainly complicated by other structural factors, most notably the angle  $\gamma$ . A preference for the  $\gamma^+$  rotamer is an important determinant in adopting a proper fit to the enzyme. In fact, it was shown earlier that the 2'- or 3'-hydroxyl groups were not essential for binding ADA (see compound **3**), but the 5'-CH<sub>2</sub>OH most likely played a critical role (56, 57). It would seem that from an assessment of all the data available, an ideal substrate would be one that was similar to dAdo in molecular composition but was biased toward an N ring pucker in solution. Along these lines, we prepared 2'-dXA (**14**) by a known synthetic route (26) as an "N" dAdo surrogate. The solution conformation of **14** was indeed N ( $P = 29.6^\circ$  at 25 °C) but the  $\gamma$  angle overwhelmingly preferred the  $\gamma^+$  rotamer (>60%; only 19%  $\gamma^+$ ). Consequently, this analogue was one of the poorest substrates of the compounds tested (data not shown). Therefore, along with the undesired positioning of the 5'-OH group, the presence of a 3'-hydroxyl group with the "unnatural" ("up") stereochemistry could also contribute to the reduced binding of **14** with ADA.

**Substrates Adjust to N in the Active Site.** Our modeling data support the notion that ADA will accommodate mostly N-puckered analogues. We have modeled the active site of ADA with compounds **2**, **4**, **7**, and **8**. Several snapshots of compounds **2** and **7** with different  $\chi$ ,  $\gamma$ , and  $P$  values (in the S hemisphere) were docked into the ADA active site. In all cases, these two S-puckered compounds adjusted to an N ring pucker after short periods of dynamics simulations. The differences in the calculated energies of the complexes of ADA with **7** and **8** were mainly derived from adjustments the  $\gamma$  angles must make in the active site when the ring pucker is S, as opposed to N. This results in nonideal [based on the crystal structure coordinates of the ADA complexes (14–17)] H-bonding geometries and distances to protein residues important for optimal binding (e.g., the differences of the distance from Asp19 OD1 to the 5'-OH in  $\beta_x$  and  $\beta_{xp}$ , Table 5). It has been well documented that there is a distinct interrelationship among the various structural parameters ( $P$ ,  $\chi$ , and  $\gamma$ ) in nucleosides (21), where the interplay among functional group stereochemistry, electronegativity, orbital interactions, and steric effects all contribute to the favored ring conformation and rotamer distributions in nucleosides and nucleotides, monomers and oligomers. In this study, a general observation was that any analogue with a substituent in the "up" position is detrimental to binding in the ADA

active site (compounds **4**, **5**, **7**, **12**, and **14**). However, the physical reasons for these difference must be critically examined on a case-by-case basis.

An intriguing outlier in the group of analogues tested was ara-A (**4**). This N-disposed compound adjusted to the S conformation for steric reasons as described above. One possible explanation for ara-A to prefer a N pucker is the gauche effect between the 2'-OH and the N9 atom, which, in the N conformation, positions the H2' proton antiperiplanar to the C1–N9 bond (21). Support for this hypothesis will come from further studies of the conformational properties and the evaluation of the electronic effects that drive the pseudorotational equilibrium in ara nucleosides.

**$\alpha$ - and  $\beta$ -FddA Revisited: Why the Difference?** We initially set out to explain the distinct difference between  $\alpha$ - and  $\beta$ -FddA when they reacted with ADA. During this study, we also observed that the chemistry of the aglycon is highly affected by the position of the fluorine atom at the 2'-position in these dideoxyadenosines. During the NMR work, we observed a slow exchange of the H8 proton of the base with deuterium over the course of several weeks at pD 5.0. However, the rate of exchange was much faster for **8** than for **7**. In addition, during the synthesis of **7** and **8**, we observed that when there was a chloro group at the C6 position of the aglycon, chemical hydrolysis to the hypoxanthine was much more facile for analogues with an  $\alpha$ -fluorine in comparison to those where the fluorine was in the  $\beta$  ("up") position (data to be described elsewhere). We initially hypothesized that there must be a potent inductive effect of the 2'-fluorine atom that was geometry-dependent. We thought that in the case of compound **8**, more efficient withdrawal of electron density from the purine aromatic system would result in faster rates of nucleophilic addition or substitution at positions C6 and C8, respectively. However, we showed that there was no effect of the fluorine stereochemistry on the protonation potential of the purine, since the  $pK_a$ s of the bases in **7** and **8** were shown to be identical. We then assumed that stabilization of the ionized (protonated) form of the base was enhanced in the N conformation of the sugar ring in  $\alpha$ -FddA **8**. This is most likely a consequence of the "communication" of the furanose ring with the aglycon through the anomeric effect, which is more efficient in nucleosides with N-type sugars. The combination of the O4'–C1'–C2'–F gauche effect and the anomeric effect keeps the population of **8** at almost 100% N at 25 °C. Thus, a preorganized N conformation with an electronegative atom in the  $\alpha$ -position of C2' seems to be a desirable template with a strong C6 hydration potential, two factors that are highly favorable for binding and catalytic turnover with ADA. Additional experiments (NMR, ab initio, and quantitative SAR studies) are in progress to describe in more detail the nature of the effects we have observed herein.

**Conclusion.** In this study, we have explored the conformational properties of various natural and synthetic substrates of ADA and found that a particular ring pucker (N) is favorable for binding at the enzyme catalytic site. Although this trend can be altered by the type and stereochemistry of the functionality present on the furanose ring, one conclusion can be drawn: It appears that a sugar with a ribo- or deoxyribofuranose template acts as a scaffold for the appropriate positioning of the  $\gamma$  and  $\chi$  angles (along with the sugar functional groups) for optimum binding and

reaction at the active site. The N scaffolding is clearly superior to the S scaffold. Thus, analogues that can assume an N pucker and position the 5'-CH<sub>2</sub>OH group and purine base properly ( $\gamma^+$  and anti  $\chi$ ) will accelerate deamination of the 6-position of adenine. These data support the observations that substrates and inhibitors prefer a 3'-endo disposition (14–17), which serves to position the remaining functional groups into proper alignment for enzyme catalysis at the active site. Evidence that ring pucker is a primary determinant in recognition and turnover of substrates by ADA has come from two recent studies from our laboratory (58, 59). Employing carbocyclic nucleoside analogues that are held rigid in either an N or S conformation, we were able to prove that ADA prefers the N-type sugar pucker by ~100-fold. These studies offer direct evidence that the positioning and stereochemistry of the functional groups in the analogues presented here are not as critical for binding as is the proper (N) ring pucker, which serves as a template to align the appropriate atoms for optimum interaction with ADA.

## REFERENCES

- Kredich, N. M., and Hershsfeld, M. S. (1989) in *The Metabolic and Molecular Basis of Inherited Disease* (Scriver, C. R., Beaudet, A. L., Sly, W. S., and Valle, D., Eds.) pp 1045–1075, McGraw-Hill, New York.
- Wolfenden, R., Kaufman, J., and Macon, J. B. (1969) *Biochemistry* 8, 2412–2415.
- Evans, B. E., and Wolfenden, R. V. (1973) *Biochemistry* 12, 392–398.
- Hershsfeld, M. S., and Mitchell, B. S. (1995) in *The Metabolic and Molecular Basis of Inherited Disease* (Scriver, C. R., Beaudet, A. L., Sly, W. S., and Valle, D., Eds.) pp 1725–1768, McGraw-Hill, New York.
- Hershsfeld, M. S. (1998) *Semin. Hematol.* 35, 291–298.
- Lowe, J. K., Gowans, B., and Brox, L. (1977) *Cancer Res.* 37, 3013–3017.
- Wilson, J. M., Mitchell, B. S., Daddona, P. E., and Kelley, W. N. (1979) *J. Clin. Invest.* 64, 1475–1484.
- Gan, T. E., Daddona, P. E., and Mitchell, B. S. (1987) *Blood* 69, 1376–13180.
- Agarwal, R. P., Spector, T., and Parks, R. E. (1979) *Biochem. Pharmacol.* 26, 259–267.
- Glazer, R. I. (1980) *Cancer Chemother. Pharmacol.* 4, 227–235.
- Smyth, J. F., Prentice, H. G., Proctor, S., and Hoffbrand, A. V. (1985) *Ann. N.Y. Acad. Sci.* 451, 123–128.
- Jehn, U., Bartl, R., Dietzfelbinger, H., Vehling-Kaiser, U., Wolf-Hornung, B., Hill, W., and Heinemann, V. (1999) *Ann. Hematol.* 78, 139–144.
- Cheson, B. D. (1994) *Curr. Opin. Hematol.* 1, 268–277.
- Wilson, D. K., Rudolph, F. B., and Quioco, F. A. (1991) *Science* 252, 1278–1284.
- Sharff, A. J., Wilson, D. K., Chang, Z., and Quioco, F. A. (1992) *J. Mol. Biol.* 226, 917–921.
- Wilson, D. K., and Quioco, F. A. (1993) *Biochemistry* 32, 1689–1694.
- Wang, Z., and Quioco, F. A. (1998) *Biochemistry* 37, 8314–8324.
- Sideraki, V., Mohamedali, K. A., Wilson, D. K., Chang, Z., Kellems, R. E., Quioco, F. A., and Rudolph, F. B. (1996) *Biochemistry* 35, 7862–7872.
- Sideraki, V., Wilson, D. K., Kurz, L. C., Quioco, F. A., and Rudolph, F. B. (1996) *Biochemistry* 35, 15019–15028.
- Saenger, W. (1984) *Principles of Nucleic Acid Structure*, Springer-Verlag, New York.
- Thibaudeau, C., and Chattopadhyaya, J. (1999) *Stereoelectronic Effects in Nucleosides and Nucleotides and Their Structural Implications*, Uppsala University Press, Uppsala, Sweden.
- Meier, C., Knispel, T., Marquez, V. E., Siddiqui, M. A., De Clercq, E., and Balzarini, J. (1999) *J. Med. Chem.* 42, 1615–1624.
- Marquez, V. E., Tseng, C. K.-H., Mitsuya, H., Aoki, S., Kelley, J. A., Ford, H., Roth, J. S., Broder, S., Johns, D. G., and Driscoll, J. S. (1990) *J. Med. Chem.* 33, 978–985.
- Ford, H., Jr., Siddiqui, M., Driscoll, J. S., Marquez, V. E., Kelley, J. A., Mitsuya, H., and Shirasaka, T. (1995) *J. Med. Chem.* 38, 1189–1195.
- Barchi, J. J., Jr., Marquez, V. E., Driscoll, J. S., Ford, H., Jr., Mitsuya, H., Shirasaka, T., Aoki, S., and Kelley, J. A. (1991) *J. Med. Chem.* 34, 1647–1655.
- Hansske, F., and Robins, M. J. (1983) *J. Am. Chem. Soc.* 105, 6736–6737.
- Bergmeyer, H. U. (Ed.) (1974) *Methods of Enzymatic Analysis*, Vol. 1, p 426, Academic Press, Inc., New York.
- Albert A., and Serjeant, E. P. (1962) *Ionization Constants of Acids and Bases*, Wiley and Sons Inc., New York.
- Van Wijk, J., Huckriede, B. D., Ippel, J. H., and Altona, C. (1992) *Methods Enzymol.* 211, 286–306 and references therein.
- Donders, L. A., de Leeuw, F. A. A. M., and Altona, C. (1989) *Magn. Reson. Chem.* 27, 556–563.
- Barchi, J. J., Jr., Jeong, L.-S., Siddiqui, M. A., and Marquez, V. E. (1997) *J. Biochem. Biophys. Methods* 34, 11–29.
- Erion, M. D., and Reddy, M. R. (1998) *J. Am. Chem. Soc.* 120, 3295–3304.
- Frisch, M. J., Trucks, G. W., Schlegel, H. B., Gill, P. M. W., Johnson, B. G., Robb, M. A., Cheeseman, J. R., Keith, T. G., Petersson, A., Montgomery, J. A., Raghavachari, K., Al-Laham, M. A., Zakrzewski, V. G., Ortiz, J. V., Foresman, J. B., Peng, C. Y., Ayala, P. Y., Chen, W., Wong, M. W., Andres, J. L., Replogle, E. S., Gomperts, R., Martin, R. L., Fox, D. J., Binkley, J. S., Defrees, D. J., Baker, J., Stewart, J. P., Head-Gordon, M., Gonzalez, C., and Pople, J. A. (1995) *Gaussian 94* (Revision B.3), Gaussian Inc., Inc., Pittsburgh, PA.
- Haasnoot, C. A. G., de Leeuw, F. A. A. M., de Leeuw, H. P. M., and Altona, C. (1979) *Recl. Trav. Chim. Pays-Bas* 98, 576.
- Rosemeyer, H., Tóth, G., Golankiewicz, B., Kazimierczuk, Z., Bourgeois, W., Kretschmer, U., Muth, H.-P., and Seela, F. (1990) *J. Org. Chem.* 55, 5784–5790.
- Plavec, J., Tong, W., and Chattopadhyaya, J. (1993) *J. Am. Chem. Soc.* 115, 9734–9746.
- Thibaudeau, C., Plavec, J., and Chattopadhyaya, J. (1996) *J. Org. Chem.* 61, 266–286.
- Bunick, G., and Voet, D. (1974) *Acta Crystallogr. B* 30, 1651–1660.
- Remin, M., Darzynkiewicz, E., Ekiel, I., and Shugar, D. (1976) *Biochim. Biophys. Acta* 435, 405–416.
- Phillips, L., and Wray, V. (1973) *J. Chem. Soc. Chem. Commun.*, 90.
- Murcko, M. A., and Dipaola, R. A. (1992) *J. Am. Chem. Soc.* 114, 10010.
- Thibaudeau, C., Plavec, J., and Chattopadhyaya, J. (1994) *J. Am. Chem. Soc.* 116, 8033–8037.
- Plavec, J., Koole, L. H., Sandström, A., and Chattopadhyaya, J. (1991) *Tetrahedron* 47, 7363–7376.
- Alberty, R. A., Smith, R. M., and Bock, R. M. (1951) *J. Biol. Chem.* 193, 425–434.
- Tate, M. E. (1981) *Biochem. J.* 195, 419–426.
- Sato, T. (1984) *Acta Crystallogr. C* 40, 880.
- Liaw, Y., Gao, Y., Marquez, V., and Wang, A. H.-J. (1992) *Nucleic Acid Res.* 20, 459–465.
- Carrera, C. J., Saven, A., and Piro, L. D. (1994) *New Drug Ther.* 8, 357–381.
- Cheson, B. D. (1998) *Semin. Hematol.* 35, 14–21.
- Thibaudeau, C., Plavec, J., Garg, N., Papchikhin, A., and Chattopadhyaya, J. (1994) *J. Am. Chem. Soc.* 116, 4038–4043.
- Plavec, J., Thibaudeau, C., and Chattopadhyaya, J. (1994) *J. Am. Chem. Soc.* 116, 6558–6560.



52. Plavec, J., Garg, N., and Chattopadhyaya, J. (1993) *J. Chem. Soc., Chem. Commun.* 12, 1011.
53. Plavec, J., Koole, L. H., and Chattopadhyaya, J. (1992) *J. Biochem. Biophys. Methods* 25, 253–272.
54. Seela, F., Debelak, H., Reuter, H., Kastner, G., and Mikhailopulo, A. (1999) *Tetrahedron* 55, 1295–1308.
55. de Leeuw, H. P. M., Haasnoot, C. A. G., and Altona, C. (1980) *Isr. J. Chem.* 20, 108–126.
56. Frederiksen, S. (1966) *Arch. Biochem. Biophys.* 113, 383–388.
57. Marrone, T. J., Straatsma, T. P., Briggs, J. M., Wilson, D. K., Quirocho, F. A., and McCammon, J. A. (1996) *J. Med. Chem.* 39, 277–284.
58. Marquez, V. E., Russ, P., Alonso, R., Siddiqui, M. A., Hernandez, S., George, C., Nicklaus, M. C., Dai, F., and Ford, H., Jr. (1999) *Helv. Chim. Acta* 82, 2119–2129.
59. Marquez, V. E., Russ, P., Alonso, R., Siddiqui, M. A., Shin, K.-J., George, C., Nicklaus, M. C., Dai, F., and Ford, H., Jr. (1999) *Nucleosides Nucleotides* 18, 521–530.

BI992112C